Journal of Dynamics, Monitoring and Diagnostics, 2025, 4, 91-100
https://doi.org/10.37965/jdmd.2025.690

ISTP
RESEARCH ARTICLE

Actuator Fault Diagnosis of 3-PR(P)S Parallel Robot Based on Dung Beetle Optimization-Back Propagation Neural Network

Junjie Huang,[1] Chenhao Huangfu,[1] Qinlei Zhang,[1,2] Shikai Li,[1] Yonggang Yan,[1] and Jiangkun Cai[1]

[1]School of Mechanical and Power Engineering, Henan Polytechnic University, Jiaozuo, China
[2]Chery Intelligent Automobile Technology (Hefei) Co, Ltd, Hefei, China

(Received 31 October 2024; Revised 11 March 2025; Accepted 02 April 2025; Published online 02 April 2025)

Abstract: Any malfunctions of the actuators of the robots have the potential to destroy the robot's normal motion, and most of the current actuator fault diagnosis methods are difficult to meet the requirements of simplifying the actuator modeling and solving the difficulty of fault data collection. To solve the problem of real-time diagnosis of actuator faults in the 3-PR(P)S parallel robot, the model of 3-PR(P)S parallel robot and data-driven-based method for the fault diagnosis are presented. Firstly, only the input-output relationship of the actuator is considered for modeling actuator faults, reducing the complexity of fault modeling and reducing the time consumption of parameter identification, thereby meeting the requirements of real-time diagnosis. A Simulink model of the electromechanical actuator (EMA) was constructed to analyze actuator faults. Then the short-term analysis method was employed for collecting the sample data of the slider position on the test platform of the EMA system and feature extraction. Training samples for neural networks are obtained. Furthermore, we optimized the Back Propagation (BP) neural network using the Dung Beetle Optimization Algorithm (DBO), which effectively resolved the weights and thresholds of the BP neural network. Compared to BP and Particle Swarm Optimization (PSO)-BP, the DBO-BP has better convergence, convergence rate, and the best-classifying quality. So, the classification for the different actuator faults is obviously improved. Finally, a fault diagnosis system was designed for the actuator of the 3-PR(P)S parallel robot, and the experimental results demonstrate that this system can detect actuator faults within 0.1 seconds. This work also provides the technical support for the fault-tolerant control of the 3-PR(P)S Parallel robot.

Keywords: actuator; Back Propagation neural network; Dung Beetle Algorithm; fault diagnosis; 3-PR(P)S parallel robot

I. INTRODUCTION

Parallel robots have the advantages of high stiffness, strong load-bearing capacity, and high motion accuracy [1,2]. It is widely used in the fields of medical equipment [3] and aerospace [4]. In harsh operating environments or amidst significant disturbances, various faults can emerge within the parallel robots. These faults can hinder the performance of a parallel robot, possibly leading to system failure or even casualties. The faults in parallel robots primarily arise from both the mechanical body and the control system. As the actuator is the weakest part of the control system, it's imperative to promptly diagnose its faults to enhance the overall reliability of the parallel robots [5].

To improve the performance and the reliability of parallel robots, and to satisfy safety and environmental requirements, research and developments in the field of actuator fault diagnosis have been continuously progressing during the last decades. The fault diagnostic methods mainly contained the model-based methods [6,7] and the data-driven methods [8]. The most used model-based method is focused on state estimation, which achieves fault isolation by building the model of the controlled object, constructing a state observer, and obtaining the residual by comparing the actual output of the system with the output of the observer. Rahme [9] proposed an adaptive sliding mode observer for the actuator fault diagnosis in linear parameter-changing systems. The main advantage is its ability to handle the time-varying distribution matrices. Xu [10] used an infinite dimensional observer, which was related to the coupling parameter updating law to diagnose the actuator faults with the dead zone nonlinearity. Zhu [11] aimed at the discrete systems with the actuator faults. The state equation affected by the external disturbances is built. The design method of reduced-order observers and the interval estimation method based on the theory of polytope were studied. So, the actuator fault detection method based on interval estimation was proposed. However, while model-based methods apply to linear systems, it is difficult to construct an accurate model of nonlinear systems due to time-varying disturbances and complex structures.

The data-driven methods have been widely used in recent years owing to adaptively extracting fault features and learning fault symptoms from large amounts of monitoring data without establishing an accurate mathematical model for the system, and the errors caused by human intervention are reduced. Chen [12] combined the fuzzy theory with the Back Propagation (BP) neural network to solve the limitations of the neural network in the fault diagnosis and applied it to the actuator fault diagnosis. Guo [13] proposed a new fault diagnosis method for the dynamic flight state of the UAV actuators based on the uncertainty-aware LSTM (UA LSTM), which has superiority in detecting the actuator faults under dynamic flight

Corresponding author: Junjie Huang (e-mail: anny@hpu.edu.cn).

conditions. Li [14] tested the proposed actuator fault detection method based on the extreme learning machines, on the self-made propeller system experimental platform. The result showed that the method was sensitive and effective in both large and small fault situations. Hou [15] improved the deep forest diagnosis method for the electric actuator fault, and the difficult parameter adjustment in existing diagnosis methods was solved. Wang [16] proposed a diagnosis algorithm based on evidence fusion, which can effectively learn the fault data features of actuators in closed-loop systems. This can improve the diagnostic capabilities and overcome the single-method misjudgment. However, the data-driven methods typically require a large amount of data to train models, which may be difficult to obtain in certain fields.

The actuator fault diagnosis methods discussed earlier have shown some progress, but most struggle to meet the requirement of concurrently simplifying actuator modeling and addressing the difficulty of collecting fault data. Therefore, a model and data-driven-based method for fault diagnosis in the actuator of a 3-PR (P) S parallel robot is put forward in this paper. Firstly, the single-fault mathematical models of the actuator are developed by solely considering the input-output relationship of the actuator (motor) speed, and the actuator faults are considered in the Simulink model of the electromechanical actuator (EMA) for analysis. Then the test platform of the EMA is built, and data on the slider position under various actuator faults are collected. Subsequently, a short-term analysis method is applied to extract fault features. The BP neural network optimized by the Dung Beetle Algorithm (DBO-BP) is employed for actuator fault classification. Ultimately, a diagnostic system for actuator faults is established in LABVIEW, which is then subjected to real-time diagnostic testing. In this paper, a fault diagnosis method for the actuator of the 3-PR(P)S parallel robot based on both model and data-driven approaches is proposed. This method simplifies the complexity of the model by considering the input-output relationship separately and solves the difficulty of obtaining fault data. The real-time fault diagnosis of the actuator is realized.

II. FAULT ANALYSIS OF THE ACTUATOR

A. 3-PR(P)S PARALLEL ROBOT

The physical platform and structural diagram of the 3-PR(P)S parallel robot [17] are shown in Fig. 1. The ontology structure of the 3-PR(P)S parallel robot is composed of the moving platform $B_1B_2B_3$ and the three branching chains $C_iA_iB_i$ $(i = 1,2,3)$ evenly distributed on the fixed platform $C_1C_2C_3$. The slider $A_i(i = 1,2,3)$ on each branching chain is linked with the column through the prismatic pair, and it is connected with the length-variable connecting rod A_iB_i $(i = 1,2,3)$ by the revolute pair. The other end of the connecting rod A_iB_i is linked with the moving platform $B_1B_2B_3$ by the spherical pair. The position and pose of the moving platform are controlled by adjusting the position of the three sliders.

As shown in Fig. 2, the EMA, which is composed of the motor (referred to uniformly as the actuator later in the paper), the ball screw, and the slider, is regarded as the driving component of the 3-PRS parallel robot.

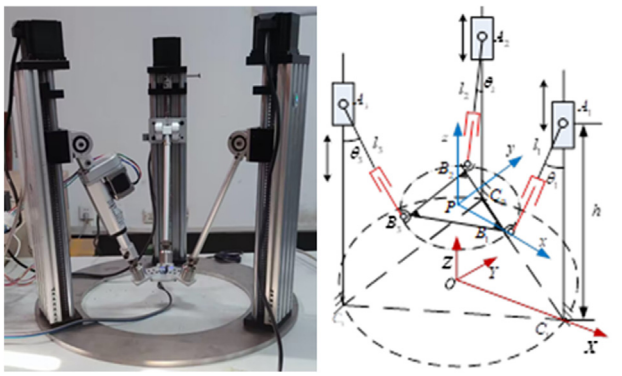

Fig. 1. 3-PR(P)S parallel robot. (a) The physical platform. (b) The structure diagram.

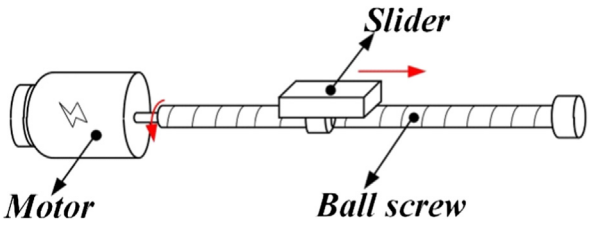

Fig. 2. Diagram of the electromechanical actuator.

B. TYPES OF THE ACTUATOR FAULTS

In practical work, the failure of the internal transmission system of the actuator (motor), damage to bearings, or jamming may lead to an abnormal increase in the actuator (motor) speed. If the internal coils and brushes of the actuator (motor) are damaged or the load exceeds the design capacity range of the actuator (motor), the actuator (motor) may fail to attain the anticipated speed. As this article mainly focuses on the study of actuator faults that affect the movement of the slider and moving platform, the emphasis is placed solely on the relationship between the input and output speeds of the actuator for the fault modeling, without considering its internal operating principles. The expression of the actuator faults is as follows:

$$U_R(t) = (1 - \rho) \cdot u(t) + f(t) \tag{1}$$

Where $U_R(t)$ represents the output speed of the actuator; $u(t)$ is the rated input speed of the actuator; ρ represents the coefficient of lost efficiency, within the range $[0,1]$; and $f(t)$ is the deviation value.

The expression varies based on the different types of actuator faults, as outlined below:

$U_R(t) = u(t)$ when $\rho = 0$ and $f(t) = 0$. The actuator is not faulty;

$U_R(t) = (1 - \rho)u(t)$ when $0 < \rho < 1$ and $f(t) = 0$. The actuator partially loses efficiency, and the fault degree increases with the increase of ρ. A linear relationship exists between the output speed and the input speed.

$U_R(t) = u(t) + C$ when $\rho = 0$ and $f(t) = C$ ($C$is a constant value). The constant-deviation fault arises in the actuator, causing a constant deviation of value C between the output and the input speed.

$U_R(t) = 0$ when $\rho = 1$ and $f(t) = 0$. The stuck fault occurs in the actuator, and the output speed is 0.

C. SIMULATION OF ACTUATOR FAULTS

A simulation model for the EMA (Fig. 3) is established in Simulink, assuming that faults solely originate from the actuator. Variations in actuator speed due to different faults will influence the position changes of the slider. Therefore, the stuck fault, the 20% efficiency-loss fault, the 40% efficiency-loss fault, and the 1 mm/s constant-deviation fault are injected into the Simulink model of the EMA and the position change of the slider is analyzed. The input speed is set as $V = 1.5\pi \cdot cos(0.5\pi \cdot t)$ and converted into the pulse signal, which is inputted into the Simulink model. The simulation time is set to $4s$. The EMA experienced the aforementioned actuator faults at $t = 3s$.

From Fig. 4, it's evident that the position curves of the slider coincide before the actuator malfunctions. When the actuator becomes stuck, an abrupt shift in the output speed to 0 occurs, leading to a cessation of slider position changes. The partial loss of efficiency in the actuator causes a reduction in its output speed, consequently leading to a slowed-down rate of position change compared to the scenario without faults. The occurrence of the constant-deviation fault prompts a sudden rise in the actuator's output speed by a positive constant, leading to a faster change in position compared to the situation without faults. It is concluded if the position deviation of the slider solely arises from distinct single faults of the actuator, the slider's position change can effectively reflect different types of actuator faults. Therefore, the actuator fault diagnosis of the 3-PR(P)S parallel robot can be regarded as the analysis of the slider position.

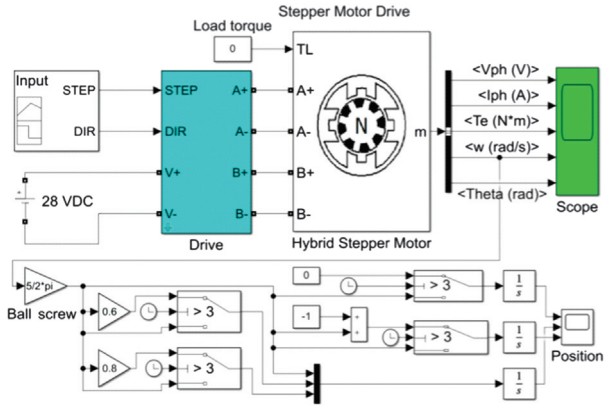

Fig. 3. Fault simulation model.

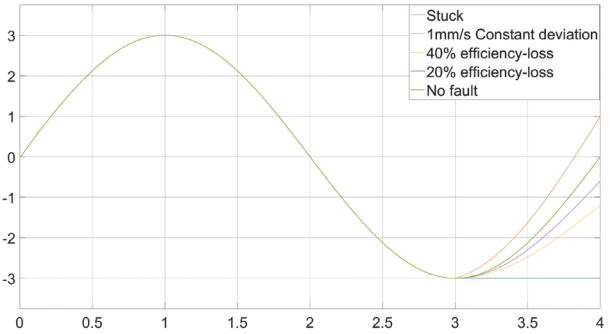

Fig. 4. Position curves of the slider.

III. FAULT DIAGNOSIS ALGORITHM FOR THE ACTUATOR

A. BACK PROPAGATION NEURAL NETWORK

It is difficult to construct an accurate model of nonlinear systems due to the time-varying disturbances and the complex structure of nonlinear systems. Because the 3-PR(P)S parallel robot is a nonlinear system, the model-based fault diagnosis method is not suitable for the 3-PR(P)S parallel robot. Therefore, a model and data-driven-based method for fault diagnosis in the actuator of a 3-PR(P)S parallel robot is put forward in this paper.

The BP neural network is a widely used artificial neural network model for solving classification and regression problems [18,19]. The application of BP neural networks proves it to be a viable approach for detecting and diagnosing actuator faults. Its basic structure is shown in Fig. 5.

The BP neural network is comprised of the input layer, the hidden layer, and the output layer. A properly functioning BP neural network includes two primary processes [20]: the forward propagation of signals and the backward propagation of errors. The BP neural network relies on the gradient descent algorithm to minimize the error between the predicted output and the actual target. This is achieved by continuously adjusting the network parameters throughout the training process.

But, when the BP neural network is applied to fault diagnosis, there are some defects, which mainly include three aspects:

(1) Uncertainty of initial weights and thresholds.

(2) It is easy to fall into local optimal values.

(3) There is no effective hidden layer node selection method.

B. DBO (THE DUNG BEETLE ALGORITHM) - BP MODEL

The improper setting of the initial thresholds and weights of the BP neural network can result in the network getting stuck in local optima, reducing the convergence speed [21]. The DBO algorithm is a biological optimization algorithm inspired by dung beetle behavior. To enhance classification accuracy and expedite convergence, the research is focused

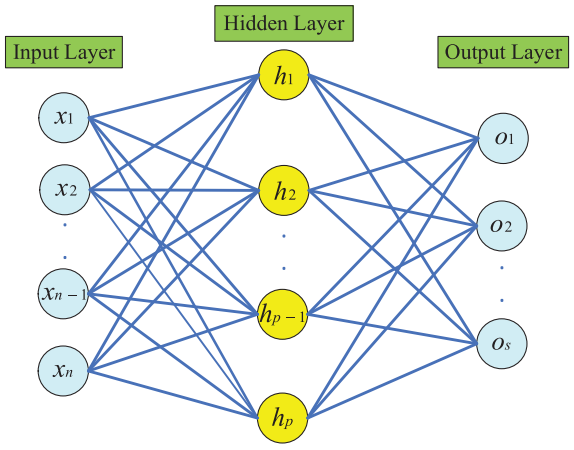

Fig. 5. The basic structure of Back Propagation neural network.

on employing the Dung Beetle algorithm [22] to optimize the initial weights and thresholds of the BP neural network. The specific steps are as follows:

Step 1: Initialize the BP neural network. The initial parameters of the network are determined. In the process of determining the hidden layer nodes, the general empirical formula is $p = \sqrt{m+n} + q$. m and n represent the number of nodes in the input and output layers, respectively, determined by the dimensionality of the sample input, $q \in [1{\sim}10]$. In numerous experiments and practical applications, it has been observed that the optimal number of hidden layer nodes typically falls within the following range [23]:

$$a = \frac{m+n}{2} \le p \le (m+n) + 10 = b \tag{2}$$

Where a is the minimum number of the hidden layer nodes, and b is the maximum number of the hidden layer nodes.

Step 2: Determine the fitness function of the DBO. The MSE (mean-square error) function is composed of the actual output T_{sim} and the predicted output T_{pre} of the BP neural network is used as the fitness function. The weights and thresholds of the network serve as the independent variables of the fitness function.

Step 3: Initialize the parameters of the dung beetle population. Multiple populations of dung beetles are randomly created and segregated into distinct groups: ball-rolling dung beetles, son dung beetles, foraging dung beetles, and thief dung beetles, following a ratio of 6:6:7:11, Subsequently, their fitness is calculated.

Step 4: The iterative optimization process updates the position of the ball-rolling dung beetle according to the following method.

No-obstacle mode:

$$x_i^{t+1} = x_i^t + a \cdot k \cdot x_i^{t-1} + b \cdot \left| x_i^t - x_{worst}^t \right| \tag{3}$$

Where t represents the number of iterations. $k \in (0,0.2)$ is a constant value that represents the deflection coefficient. $b \in (0,1)$. a is assigned either the value of 1 or –1., 1 represents the original direction, and –1 represents diverging from the original direction. x_{worst}^t is the global worst position, $|x_i^t - x_{worst}^t|$ is utilized to simulate changes in light intensity.

For the value of a, setting the probability value λ:

$$\begin{array}{c} if\ \eta > \lambda \quad \left(0 < \eta < 1\right) \\ a = 1 \\ else \\ a = 1 \end{array} \tag{4}$$

Obstacle mode:

$$x_i^{t+1} = x_i^t + \tan(\theta) \cdot \left| x_i^t - x_i^{t-1} \right| \tag{5}$$

Step 5: During the iterative optimization process, the update process for the birth position of the son dung beetle is as follows.

$$B_i^{t+1} = x_{gbest}^t + b1 \cdot (B_i^t - Lb*) + b2 \cdot (B_i^t - Ub*) \tag{6}$$

Where b_1, b_2 are the two different independent random vectors with the size of $1 \times D$, and D is the dimension of the optimization variables.

The son dung beetles need to obey the following boundary rule during the process of being given birth.

$$\begin{cases} Lb* = \max\left\{ x_{gbest}^t \cdot (1-R), Lb \right\} \\ Ub* = \min\left\{ x_{gbest}^t \cdot (1+R), Ub \right\} \end{cases} \tag{7}$$

Where $R = 1 - \frac{t}{T_{max}}$, Ub and Lb are the upper and lower bounds of the optimization problem, respectively.

Step 6: During the iterative optimization process, the method for updating the position of the foraging dung beetle is as follows.

$$x_i^{t+1} = x_i^t + C1 \cdot |x_i^t - Lb^l| + C2 \cdot |x_i^t - Ub^l| \tag{8}$$

Where $C1$ represents a randomly generated number following the normal distribution. $C2$ is a random vector belonging to the range of (0, 1), with the dimensions of $1 \times D$.

Similarly, the foraging dung beetles also need to obey the following boundary rule:

$$\begin{cases} Lb^l = \max\left\{ x_{gbest}^t \cdot (1-R), Lb \right\} \\ Ub^l = \min\left\{ x_{gbest}^t \cdot (1+R), Ub \right\} \end{cases} \tag{9}$$

Step 7: During the iterative optimization process, the method for updating the position of the thief dung beetle is as follows.

$$x_i^{t+1} = x_{lbest}^t + S \cdot g\left(\left| x_i^t - x_{gbest}^t \right| + \left| x_i^t - x_{lbest}^t \right| \right) \tag{10}$$

Where S is a constant value. g is a random vector with the dimensions of $1 \times D$, which obeys the normal distribution.

Step 8: Start the iterative optimization and update the location of dung beetles. Find the position of the dung beetle corresponding to the optimal fitness value, which is the optimized initial weights and the thresholds.

Step 9: Reinitialize the initial weights and thresholds of the network.

Step 10: Train the BP neural network to obtain the training results, and the network is tested. The overall flowchart is shown in Fig. 6

IV. EXPERIMENTS AND SIMULATIONS

A. DATA ACQUISITION AND FEATURE EXTRACTION

According to the test requirements, this paper builds a test platform for the EMA system and the specific structure is shown in Fig. 7. The speed command $V = 1.5\pi \cdot cos(0.5\pi \cdot t)$ is inputted to the EMA. The linear encoder is employed to separately collect the position data of the slider when the actuator is in the no-fault, the stuck fault, the 20% efficiency-loss fault, the 40% efficiency-loss fault, and the 1 mm/s constant-deviation fault modes. The sampling period is $T = 4s$ and the sampling frequency is 50 HZ. The sensor used is a DC11 linear grating ruler with a measuring range of 150 mm, an accuracy of 1um, and a resolution of 0.1 um.

Due to the evolving feedback position data over time, notable discrepancies exist in the position data captured at

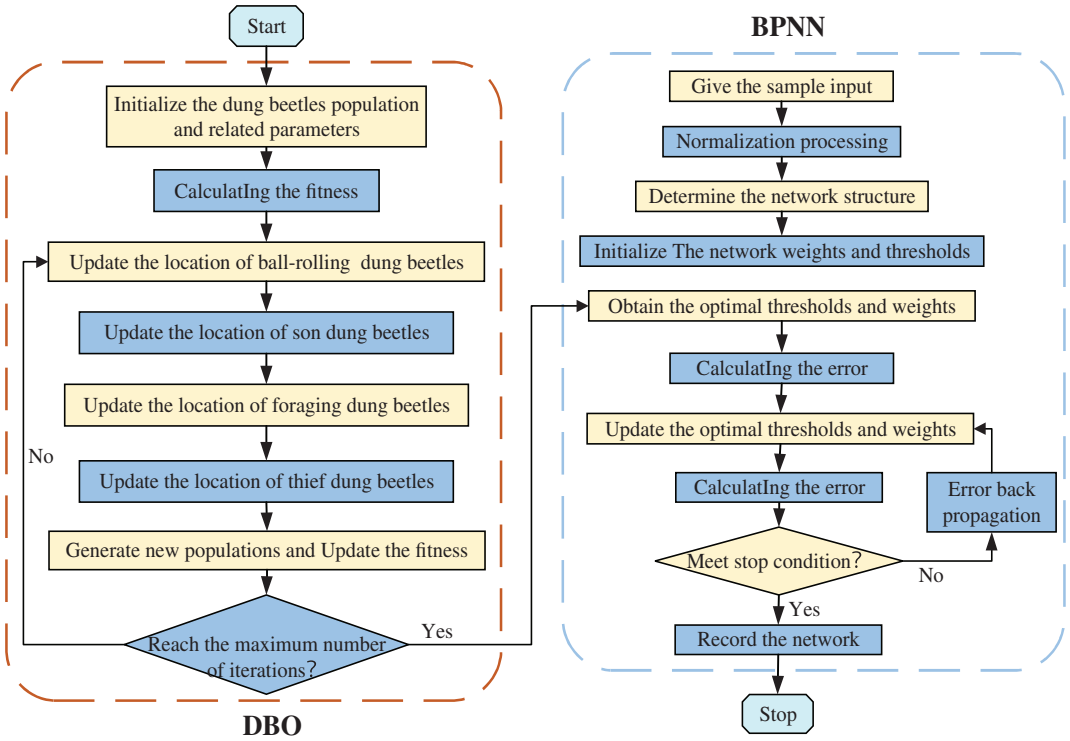

Fig. 6. The Flowchart of Dung Beetle Optimization-Back Propagation model.

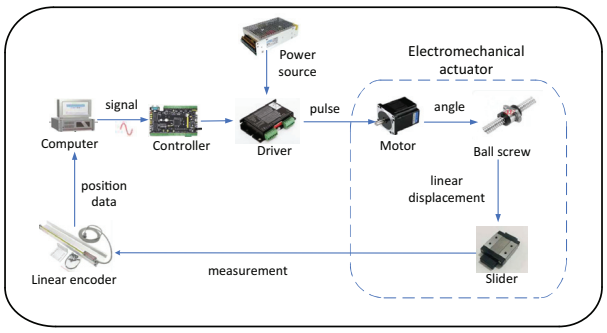

Fig. 7. The test platform of the electromechanical actuator system.

different points in time, so the method of short-term analysis [24] is introduced. The sampling period $T = 4s$ is segmented into K frames with equal lengths t, each frame contains l position data. Given the necessity for subsequent real-time fault diagnosis experiments on the upper computer, the speed of running the neural network model in LABVIEW was assessed, yielding a minimum result of 0.06s, which means running once needs at least $0.06s$, so frame length is taken as $t = 0.1s$, $K = 40$ and $l = 5$. Set 40 fault time point within the $0{\sim}4s$ timeframe, spaced at intervals of $0.1s$.

Firstly, gather 20 sets of slider's position data under no-fault mode, with each set comprising 200 data. Segment each set of position data into 40 frames, resulting in 800 (20×40) no-fault position samples. Subsequently, gather 20 sets of position data when an actuator fault happens at a specified fault time point, and take the position data of the frame at that time point. Within a sampling period, comprising 40 fault time points, 800 (40×20) fault position samples are acquired for a type of actuator fault. As a result of four different actuator faults, 3200 (4×40×20) fault position-samples were obtained. In a total, 4000 position samples were obtained. (no fault position-samples and fault position-samples).

The time domain features can well reflect the distribution characteristics of the position data over some time. Consequently, the feature of each position sample is comprised of the Average Value, Variance, Root Mean Square, Absolute Average, Peak-Peak of this position sample, and the ending time $t(i)$ of the frame corresponding to this position-sample:

$$Ei = [Mean(i), Var(i), Rms(i), Av(i), Pk(i), t(i)]^T \quad (11)$$

Where,

$$Mean(i) = \frac{\sum_{p=1}^{l_1} \cdot S(p)}{l_1} \quad (12)$$

$$Var(i) = \frac{1}{l_1 - 1} \cdot \sum_{p=1}^{l_1} (S(p) - \bar{S})^2 \quad (13)$$

$$Rms(i) = \sqrt{\frac{1}{l_1} \cdot \sum_{p=1}^{l_1} (S(p))^2} \quad (14)$$

$$Av(i) = |Mean(i)| \quad (15)$$

$$Pk(i) = Max(S(p)) - Min(S(p)) \quad (16)$$

$$t(i) = 0.1 * i \quad (17)$$

Where s represents the value of the position data, $i \in 1{\sim}40$.

A total of 4000 sets of feature samples were obtained.

B. SAMPLE DIVISION AND NORMALIZATION

The sample input of the BP neural network consists of 4000 sets of feature samples. The fault labels corresponding to each type of fault are outlined in Table I, and the sample output of the BP neural network is formed by these labels. There are 20 samples for each type of fault at every fault time point, which are divided into training samples and testing samples at a ratio of 9:1. This results in a total of 3600 (18×5×40) training samples and 400 testing samples (2×5×40).

The sample input is normalized by using the Mapminmax function [25], and the processed sample input e is obtained:

$$e = \frac{(e_{max} - e_{min})(E - E_{min})}{E_{max} - E_{min}} + e_{min} \tag{18}$$

where E is the sample input. E_{max}, E_{min} represent the maximum and minimum values of E, respectively. e is the normalized sample input. e_{max}, e_{min} represent the maximum and minimum values of the sample input after normalization, which are 1 and –1, respectively.

The fault labels are normalized and converted into coding format as shown in Table II.

After the training of the neural network is completed, the output fault labels need to be anti-normalized.

C. PARAMETER SETTING OF DBO-BP

- Parameter Initialization of the DBO. The number of beetles in the DBO is $pop = 30$. The number of iterations is $T_{max} = 50$. The searching range of the initial thresholds and the weights is $[-3,3]$.
- Parameter Initialization of the BP neural network. The sample input is the 6-dimensional data and the corresponding sample output is the 5-dimensional data, so the number of the input layer nodes is $m = 6$, and the number of the output layer nodes is $n = 5$. The learning rate c is set at 0.01. The training accuracy is set at 10^{-6}.

According to the formula 2, The range for the number of hidden layer nodes is 6~21. The BP neural network is trained using these 16 values as the number of hidden layer nodes. The training epoch is set at 100. Figure 8 displays the test results. From Fig. 8, it can be seen that the training error MSE is minimized when the number of nodes is 16, which means the convergence effect is best. Consequently, the number of hidden layer nodes is set to 16.

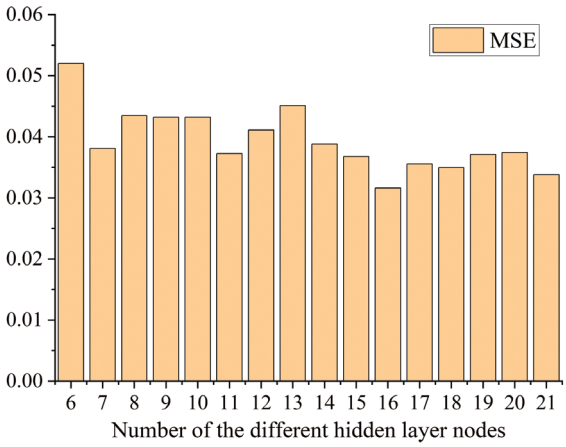

Fig. 8. Training error of different hidden layer nodes.

D. ALGORITHM COMPARISON AND RESULT ANALYSIS

In this comparison experiment, MSE is taken as the loss function, and the same samples are used to train and test the BP, PSO-BP (the BP Neural Network Optimized by Particle Swarm Optimization Algorithm) and DBO-BP models separately. The training and testing results are shown in Fig. 9 and the comparative results are depicted in Fig. 10 and Table III.

From Fig. 9(a), it's evident that as the training progresses, the MSE of all algorithms continuously decreases and converges. Figure 8 and Table III provide a comparative analysis of the performance among the three algorithms. The BP, PSO-BP, and DBO-BP have been trained for 146 epochs, 85 epochs, and 66 epochs, respectively. The DBO-BP has the best MSE, which means it has better convergence and convergence rate. The corresponding classification accuracies are 90%, 94.75%, and 97.75%, respectively. The DBO-BP has the best-classifying quality. Therefore, the DBO-BP model can effectively classify the different actuator faults.

V. REAL-TIME DIAGNOSTIC TESTING OF ACTUATOR FAULTS

A. REAL-TIME DIAGNOSTIC SYSTEM

The real-time diagnosis system is designed based on the upper computer software LabView, which consists of the data acquisition module and the fault diagnosis module.

Table I. The fault labels

Fault type	No fault	Stuck	20% efficiency-loss	40% efficiency-loss	1 mm/s constant-deviation
Label	1	2	3	4	5

Table II. The normalized fault labels

Fault type	No fault	Stuck	20% efficiency-loss	40% efficiency-loss	1 mm/s constant-deviation
Label	[1,0,0,0,0]	[0,1,0,0,0]	[0,0,1,0,0]	[0,0,0,1,0]	[0,0,0,0,1]

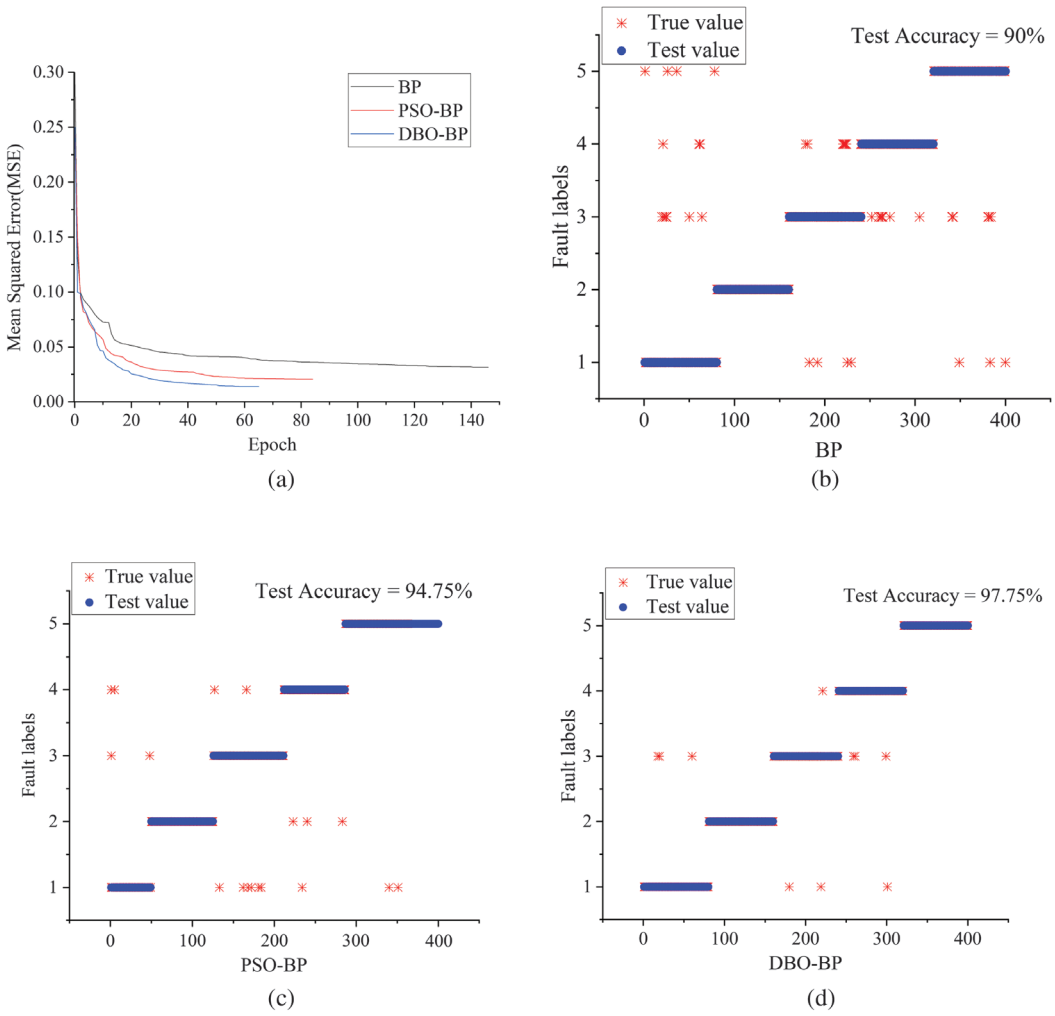

Fig. 9. Training and testing results: (**a**) The training error of Back Propagation (BP), Particle Swarm Optimization (PSO)-BP, and Dung Beetle Optimization-Back Propagation (DBO-BP). (**b**) The classification accuracy of BP (**c**) The classification accuracy of PSO-BP. (**d**) The classification accuracy of DBO-BP.

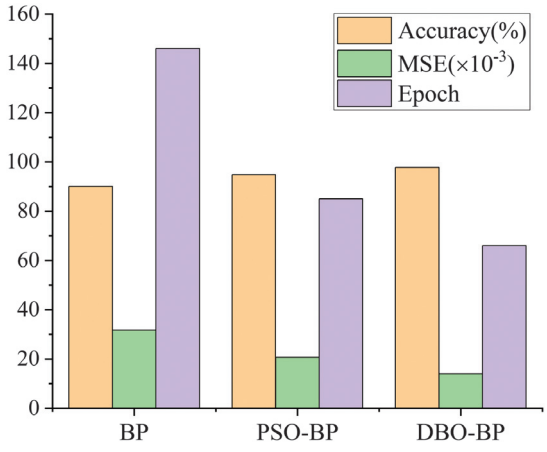

Fig. 10. The comparison of Back Propagation (BP), Particle Swarm Optimization (PSO)-BP, and Dung Beetle Optimization-BP.

The data acquisition module must establish communication between STM32 and LabView. In order to reflect the data characteristics of each time period, it is necessary to collect enough data. Therefore, the sampling interval is configured at 20 ms, and a sliding array is added to capture and store the real-time position data of each frame, then the display of real-time curve display is performed on the collected position data.

In the fault diagnosis module, the time-domain features of the sliding window array are calculated and the trained DBO-BP model is integrated into the MATLAB script function. The Boolean signal light is used to display the fault status according to the output result of the DBO-BP model. The diagnosis frequency is 10 Hz.

B. THE REAL-TIME FAULT DIAGNOSIS EXPERIMENT OF ACTUATOR

The proposed scheme is applied to the 3-PR(P)S redundant parallel manipulator (Seen in Fig. 1) to demonstrate the effectiveness of the strategy. Before the experiment, the LABVIEW program should be connected with the STM32 controller, and the parameters are set. The motor is 57BYG250B-8 stepper motor, the stepping Angle is 1.8°, the number of phases is 2, and the encoder resolution is 64. The driver selected is the DM542 stepper motor driver. The actuator fault diagnosis module of the control system is designed to detect different actuator faults at the time points.

The process of experiment is as follows:

Table III. The comparison of BP, PSO-BP, and DBO-BP based on same samples

Diagnosis algorithm	Iterations (MSE)	Training error	Accuracy
BP	146	0.03161	90%
PSO-BP	85	0.02064	94.75%
DBO-BP	66	0.01397	97.75%

1. Firstly, given the end trajectory, the position equation for shaft is obtained by the inverse kinematics equation of the actuator faults.
2. The sampling period is set to $T = 4s$. The selected fault time points are randomly selected: $t_1 = 0.5s$, $t_2 = 1.6s$, $t_3 = 2.2s$ and $t_4 = 3.6s$.
3. Then, the jam fault, the 20% failure state of the actuator, the 40% failure state of the actuator, and 1 mm/s constant deviation fault at each selected fault time are experimented with and finished.
4. Finally, the actuators are injected with the state of jamming, failure 20%, failure 40%, and constant deviation faults of 1 mm/s at these time points to demonstrate the effectiveness and accuracy of the fault diagnosis system.

The test results are as follows:

From Figs. 11–14, it can be known that the new fault diagnosis system constructed in this paper has a good diagnosis effect on the state of stuck fault. Simultaneously, for the diagnosis of these four fault conditions, it can be detected 0.1s after actuator failure. From the above analysis, it can be seen that the fault diagnosis system can achieve the real-time diagnosis function of actuator faults, so it has a

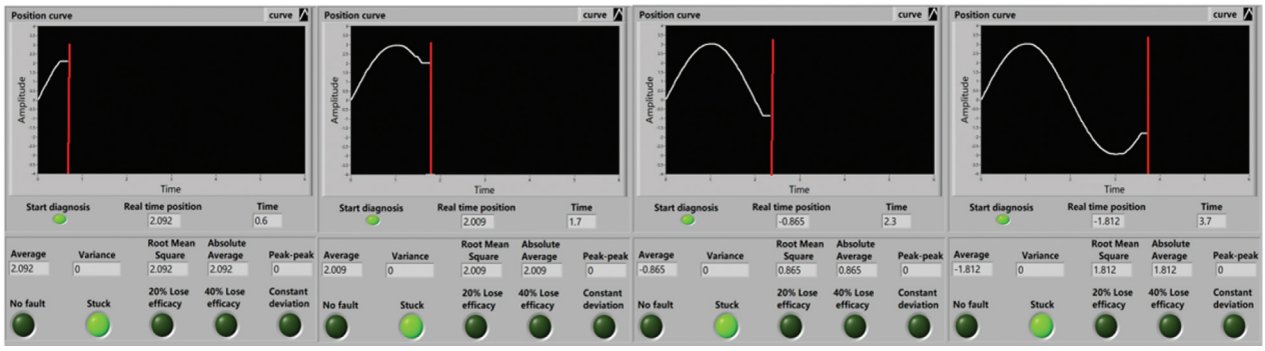

Fig. 11. Diagnostic result of stuck fault.

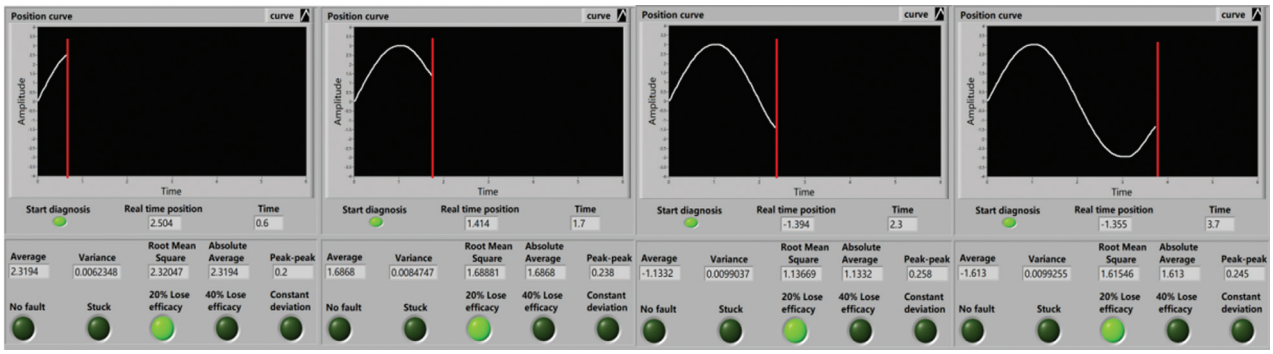

Fig. 12. Diagnostic result of 20% efficiency-loss fault.

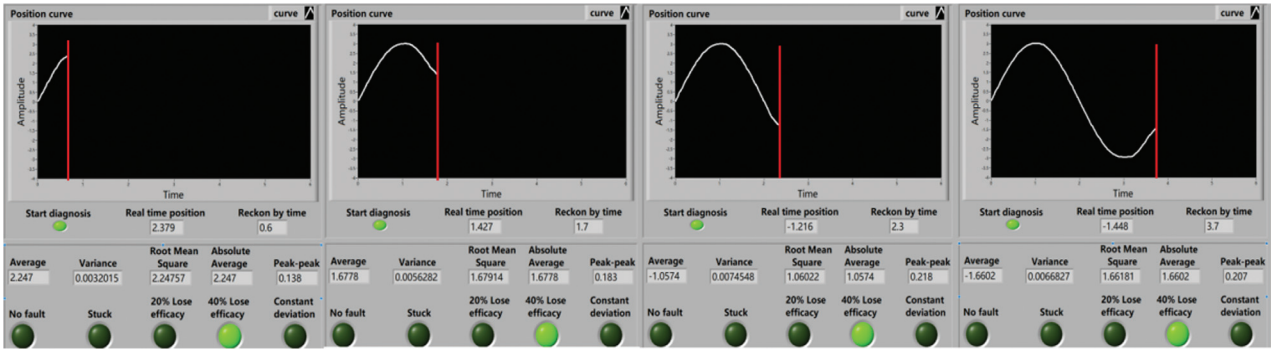

Fig. 13. Diagnostic result of 40% efficiency-loss fault.

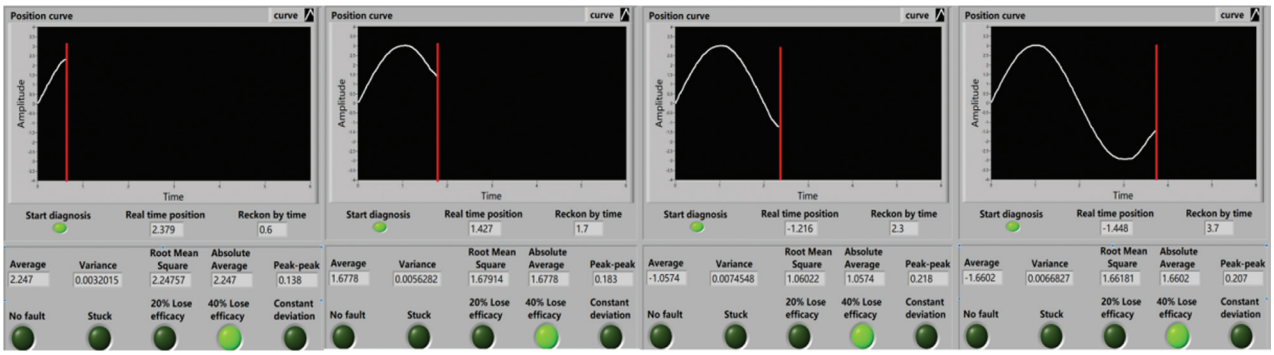

Fig. 14. Diagnostic result of 1 mm/s constant deviation fault.

certain reference significance for the subsequent diagnosis practice.

VI. CONCLUSIONS

To achieve real-time diagnosis of actuator faults, and meet the requirements of both eliminating the complexity of actuator modeling and the difficulty of data collection simultaneously, this paper proposes a model and data-driven-based method for fault diagnosis in the actuator of the 3-PR(P)S parallel robot. The following conclusions were obtained through the theoretical analysis and the experimental verification:

1) Only the input-output relationship of the actuator is taken into account for modeling actuator faults, it reduces the modeling complexity. The actuator faults are considered in the Simulink model of the EMA and analyzed, and the simulation results indicate that the position change of the slider can reflect different types of actuator faults.
2) Our study advances a more effective approach to fault diagnosis for the actuator. The data of slider position under different actuator faults are collected and the short-term analysis method is used for feature extraction. The DBO-BP model optimized the weights and thresholds in BP neural network. The experimental results indicate that the DBO-BP model outperforms BP and PSO-BP in terms of classification quality and convergence, proving particularly effective in diagnosing actuator faults.
3) To detect the actuator faults in real-time, the actuator fault diagnosis system is designed based on LabView. Through the real-time fault diagnosis experiment of actuator, the results are presented that the designed system is capable of effectively and precisely detecting actuator faults within 0.1 seconds. This proves that the developed system is correct and effective. At the same time, the system can be used in the fault diagnosis of parallel robots with similar actuators.

CONFLICT OF INTEREST STATEMENT

The authors declare no conflicts of interest.

REFERENCES

[1] P. Ye, J. You, X. Chou, L. Wang, and C. Li, "Status and development trend of motion performance in parallel robot," *J. Nanjing Univ. Aeronaut. Astronaut.*, vol. 52, pp. 363–377, 2020.

[2] C. Zhu, Z. Sun, and J. Zhang, "Accuracy synthesis of a 2UPS & UPR & UP parallel robot," *J. Mech. Transm.*, vol. 47, pp. 11–16, 2023.

[3] R. J. Escarabajal, J. L. Pulloquinga, M. Vicente, V. Ángel, and D. Miguel, "Model-based control of a 4-DOF rehabilitation parallel robot with online identification of the gravitational term," *Sensors*, vol. 23, p. 2790, 2023.

[4] B. Xu et al., "Design and research of aircraft landing gear omni-directional mobile assembly robot," *Aeronaut. Manuf. Technol.*, vol. 64, pp. 60–67, 2021.

[5] Q. Xu, C. Zheng, Q. Mai, K. Wan, and W. He, "Adaptive fuzzy learning control for systems with actuator failures and unknown control directions," *Control Eng. China*, vol. 30, pp. 1706–1719, 2023.

[6] A. Azarbani, A. Fakharian, and M. B. Menhaj, "On the design of an unknown input observer to fault detection, isolation, and estimation for uncertain multi-delay nonlinear systems," *J. Process Control*, vol. 128, p. 23, 2023.

[7] C. Wu, J. T. Qi, D. L. Song, X. Qi, and J. D. Han, "Simultaneous state and parameter estimation based actuator fault detection and diagnosis for an unmanned helicopter," *Int. J. Appl. Math. Comput. Sci.*, vol. 25, pp. 175–187, 2015.

[8] Q. Cui. *Platform Development and Fault Diagnosis Methods for Servo Motor*. Harbin: Harbin Institute of Technology, 2022.

[9] S. Rahme, N. Meskin, and J. Mohammadpour, "Adaptive sliding mode–based diagnosis of actuator faults for LPV systems," *Int. J. Adapt. Control Signal Process.*, vol. 31, pp. 1265–1272, 2017.

[10] X. D. Xu and S. Dubljevic, "Robust state estimation for positive real infinite-dimensional systems with actuator and sensor faults," *IEEE Syst. J.*, vol. 15, pp. 4887–4894, 2021.

[11] F. Z and M. L, "Actuator fault detection based on combination of reduced-order observer and zonotope method," *J. Tongji Univ. Nat. Sci.*, vol. 51, pp. 271–279, 2023.

[12] Q. Chen, L. Hou, and J. Cao, "Actuator fault diagnosis based on fuzzy neural network," *Electron. Des. Eng.*, vol. 21, pp. 105–107+110, 2013.

[13] K. Guo, N. Wang, D. T. Liu, and X. Y. Peng, "Uncertainty-aware LSTM based dynamic flight fault detection for UAV actuator," *IEEE Trans. Instrum. Meas.*, vol. 72, pp. 1–13, 2023.

[14] C. Li, Y. Zhang, and P. Li, "Extreme learning machine based actuator fault detection of a quadrotor helicopter. *Advances Mech. Eng.*, vol. 9, pp. 1–10, 2017.

[15] G. Hou, Z. Lv, W. Zhang, and K. Wu, "Fault diagnosis method of electric actuator based on improved deep forest," *Autom. Instrum.*, vol. 37, pp. 54–59, 2022.

[16] Y. Wang and T. Sun, "A method of actuator fault diagnosis based on evidence fusion," *Control Decis*, vol. 37, pp. 2026–2032, 2022.

[17] J. Huang, P. Wang, B. Zhang, and J. Zhao, "Redundancy design and workspace analysis of 3-PRS parallel mechanism," *J. Mech. Transm.*, vol. 46, pp. 25–34+41, 2022.

[18] S. S. Wu, G. F. Zhao, and B. S. Wu, "Real-time prediction of the mechanical behavior of suction caisson during installation process using GA-BP neural network," *Eng. Appl. Artif. Intell.*, vol. 116, p. 11, 2022.

[19] C. S. Yuan, X. M. Sun, and Q. M. J. Wu, "Difference co-occurrence matrix using BP neural network for fingerprint liveness detection," *Soft Comput.*, vol. 23, pp. 5157–5169, 2019.

[20] Y. H. Pan, Y. H. Wang, P. Zhou, Y. Yan, and D. M. Guo, "Activation functions selection for BP neural network model of ground surface roughness," *J. Intell. Manuf.*, vol. 31, pp. 1825–1836, 2020.

[21] L. Yang, H. Zheng, G. Luo, and L. Yang, "Retrieval of soil salinity content based on BP neural network optimized by genetic algorithm," *Geogr. Geo-Inf. Sci.*, vol. 37, pp. 12–21 +37, 2021.

[22] Z. Pan and F. Bu, "DV-Hop localization algorithm optimized based on dung beetle optimizer," *J. Electron. Meas. Instrum.*, vol. 37, pp. 1–10, 2023.

[23] K. Xia, C. Li, and J. Shen, "An optimization algorithm on the number of hidden layer nodes in feed-forward neural network," *Comput. Sci.*, vol. 32, pp. 143–145, 2005.

[24] A. Ravankar, A. A. Ravankar, Y. Kobayashi, Y. Hoshino, and C. C. Peng, "Path smoothing techniques in robot navigation: state-of-the-art, current and future challenges," *Sensors*, vol. 18, p. 3170, 2018.

[25] K. Hu, W. Luo, and S. Jia, "RON prediction model based on BP neural network," *J. Wuhan Text. Univ.*, vol. 34, pp. 27–32, 2021.